Position Periodic Control of Two Rotating Airplanes

José Antonio Bautista-Medina, Rogelio Lozano, Antonio Osorio-Cordero

drones

MDPI

Article

Position Periodic Control of Two Rotating Airplanes

José Antonio Bautista-Medina [1], Rogelio Lozano [1,2,*] and Antonio Osorio-Cordero [1]

[1] UMI LAFMIA 3175 CNRS CINVESTAV-IPN, Mexico City 07360, Mexico
[2] Heudiasyc CNRS UMR 7553, Université de Technologie de Compiègne, CEDEX, 60203 Compiègne, France
* Correspondence: rlozano@hds.utc.fr

Abstract: The increasing development in aerial vehicles shows a wide range of configurations for different requirements. Many of them combine conventional configurations' features to take advantage of their qualities, such as performing a cruise flight as an airplane and hovering like a helicopter. Thereby, this study analyzes the modeling and control of a pair of fixed-wing airplanes joined together to form a larger rotor that incorporates valuable features in missions with aerial vehicles. The model uses the Lagrange approach to obtain the motion equations in the flight plane, and two control strategies are proposed to regulate the movement in the horizontal plane: a cyclic proportional derivative control and a positive function. Both controls generate a sinusoidal signal to regulate the thrust of the motors, and this leads to the generation of pulses that direct and move the vehicle toward a desired position until it is reached. Our analysis is validated by simulation that shows how both controls govern the center of mass position of the rotating planes, and it also shows the airplanes' trajectory. The results show good performance.

Keywords: fixed-wing airplane; positive function; Unmanned Aerial Vehicle; virtual swashplate

Citation: Bautista-Medina, J.A.; Lozano, R.; Osorio-Cordero, A. Position Periodic Control of Two Rotating Airplanes. *Drones* **2022**, *6*, 214. https://doi.org/10.3390/drones6080214

Academic Editor: Mostafa Hassanalian and Abdessattar Abdelkefi

Received: 30 June 2022
Accepted: 17 August 2022
Published: 19 August 2022

1. Introduction

Unmanned Aerial Vehicles (UAVs) can be classified as fixed-wing and rotary-wing vehicles, or aircraft (A/C) and helicopters. Aircraft can fly long distances and consume much less energy than helicopters, but in contrast to aircraft, helicopters can hover. The increasing development in aerial vehicles shows a wide range of configurations for different requirements. These include vehicles that combine features of conventional configurations such as convertible aircraft [1,2]. However, the complexity of the mechanical design has negatively affected the development of convertible aircraft [3,4]. The objective of the prototype presented is to obtain a UAV that can fly as efficiently as an aircraft but can hover like a helicopter [5,6].

Convertible aircraft can facilitate lots of flight operations. The weight of the prototype presented in this paper is clearly smaller than that of an equivalent helicopter and thus leading to larger endurance. Therefore, it can replace a conventional helicopter in surveillance tasks and have more time to complete its mission successfully. The prototype is mechanically simpler than a helicopter, and this will save cost maintenance and time. Thinking of applications, in view of its longer endurance, it may be considered for use as an emergency radio relay.

This paper presents a set up of two fixed-wing rotary airplanes connected by a rigid rod. The vehicle configuration can operate efficiently as an aircraft and hover as a helicopter. In hovering flight, the two attached aircraft rotate in a circle around the center of the rigid rod attaching them. According to the proposed configuration, the airplanes are assumed to be the blades of a helicopter. The distance between airplanes depends on the length of the rigid rod that connects them. Turbulence may interfere with the efficiency of the aircraft flight when the distance between them is similar to the distance between the blades of a helicopter. With an adequate rigid rod length, the negative turbulence effects can be diminished.

Note also that in a helicopter, the engine is in the fuselage, whereas in the proposed configuration, the motors are in each airplane. Contrary to the two airplanes' configuration, a helicopter requires a swashplate, a gearbox, and a tail rotor that increase its weight [7].

There are various benefits of the proposed configuration compared to a helicopter: It does not require a tail rotor and its associated gear. A reduction gearbox does not need to be installed between the engine and the main rotors. There is no need for a mechanical swash plate. A fuselage is not required. It is mechanically simpler. In view of the reduction of weight, it should have an increased endurance, larger energy efficiency and less air turbulence compared to an equivalent helicopter. In addition, as an airplane, it may be driven by solar energy [8]. We consider that if we sufficiently separate the two rotating airplanes, they can be driven in the same way.

The modeling and control of the two rotating airplanes which form a larger rotor result in valuable characteristics in the world of aerial vehicles, which is addressed in [9]. Considering the periodic operation of the set up, positive function as well as cyclic proportional derivative (PD) control approaches have been implemented. These play the role of the swashplate in helicopters to command the displacement of the prototype in the horizontal plane.

This paper focuses on the development of the aerodynamical model of the two rotating airplanes using the Euler–Lagrange approach. Two control designs are proposed to regulate the horizontal displacement in such a way that a swashplate is virtually created. The controllers stabilize the planar position at the same time that the angular rotation is regulated. The performance of the control strategies is presented in numerical simulations.

2. System Description

This section presents a control strategy for an aerial vehicle consisting of two fixed-wing aircraft in constant rotation. The strategy is based on a conventional PD control that varies cyclically due to the aircraft dynamics. The cyclic strategy is designed to control the motion of the set up in two dimensions.

Each aircraft has two control surfaces, an elevator and a rudder. While the elevator can be used to change altitude, the rudder produces a rotational movement of the aircraft around the stick joint. This angular displacement is denoted by the angle μ and varies equally for both airplanes. To further simplify the model, it is considered that a mechanism at the junction of the wing and the rod modifies this angle. Based on this arrangement, the joint has a range of motion of $-90^\circ \leq \mu \leq 90^\circ$; therefore, the angle between the two planes is defined as

$$\mu_a = 180^\circ - 2\mu, \tag{1}$$

measured from the thrust vector T_1 toward the thrust vector T_2 in the clockwise direction. The distance between the center of mass (CM) of the whole system and the CM of each airplane is denoted by l. For this case study, the thrust vectors T_1 and T_2 are considered as control variables, while μ is considered as a disturbance.

3. Dynamic Model

3.1. Forces and Moments

The thrust forces T_1 and T_2 are expressed in the body axes as

$$\begin{bmatrix} f_x \\ f_y \end{bmatrix} = \begin{bmatrix} T_1 \cos(\mu) \\ T_1 \sin(\mu) \end{bmatrix} + \begin{bmatrix} -T_2 \cos(\mu) \\ T_2 \sin(\mu) \end{bmatrix}, \tag{2}$$

and produce a moment represented by

$$N = lT_1 \cos(\mu) + lT_2 \cos(\mu), \tag{3}$$

acting about the z-axis of the body.

3.2. Thrust Force of the Motors

The thrust force of a motor is given by

$$T = \rho n^2 D^4 C_T, \tag{4}$$

where ρ is the density of the air, n corresponds to the revolutions per second of the motor, D is the diameter of the propeller and C_T is the thrust coefficient [10]. Then, the thrust forces are defined as

$$T_1 = \rho n_1^2 D^4 C_{T_1}, \tag{5}$$

$$T_2 = \rho n_2^2 D^4 C_{T_2}, \tag{6}$$

and the motors are considered to operate under similar conditions, same density and equal propeller size. If the angular velocity of the motors is different, the thrust coefficients will also be different.

In practice, it is common to characterize the thrust force in the motors as a function of the number of revolutions. From [11], we obtain the data for a propeller of 4.5 inches in diameter; then, the function of the thrust coefficient is obtained as

$$C_T = \begin{cases} f(n) & \text{for } 1500 \leq n \leq 10800 \\ 0, & \text{otherwise} \end{cases}, \tag{7}$$

where

$$f(n) = -1.9743 \times 10^{-10} n^2 + 3.8068 \times 10^{-6} n + 0.1030, \tag{8}$$

note that the trust coefficient depends on the revolutions per second.

3.3. Translational Dynamic Equations

To develop the motion equations, the aircraft system is considered as point masses; see Figure 1.

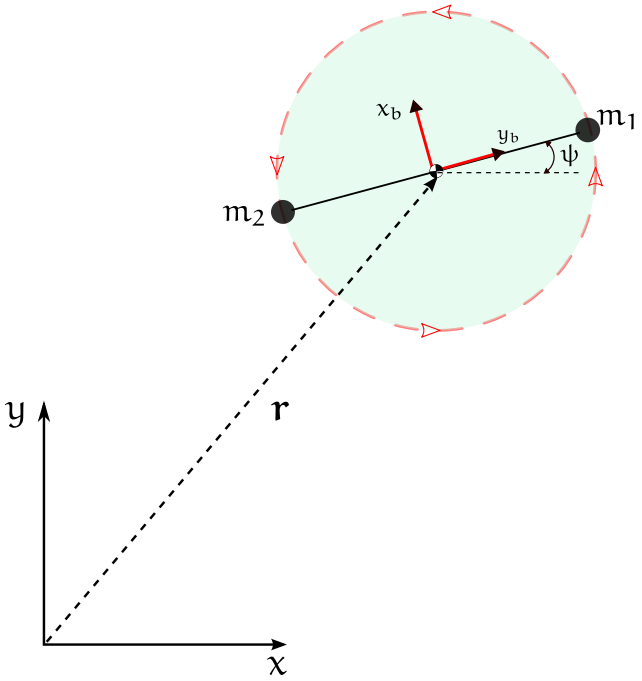

Figure 1. Top view of the system in the inertial plane.

The vector **r** goes from the inertial origin to the CM of the system, that is

$$\mathbf{r} = [x \quad y]^T, \tag{9}$$

while the position of each plane with respect to the body frame is expressed as

$$[x_1 \quad y_1]^T = [0 \quad l]^T, \tag{10}$$

$$[x_2 \quad y_2]^T = [0 \quad -l]^T, \tag{11}$$

this can also be expressed with respect to the inertial frame as

$$\begin{bmatrix} x_{m_1} \\ y_{m_1} \end{bmatrix} = \begin{bmatrix} x \\ y \end{bmatrix} + \begin{bmatrix} -\sin\psi & \cos\psi \\ \cos\psi & \sin\psi \end{bmatrix} \begin{bmatrix} 0 \\ l \end{bmatrix}, \tag{12}$$

$$\begin{bmatrix} x_{m_2} \\ y_{m_2} \end{bmatrix} = \begin{bmatrix} x \\ y \end{bmatrix} + \begin{bmatrix} -\sin\psi & \cos\psi \\ \cos\psi & \sin\psi \end{bmatrix} \begin{bmatrix} 0 \\ -l \end{bmatrix}, \tag{13}$$

where

$$R_b^i = \begin{bmatrix} -\sin\psi & \cos\psi \\ \cos\psi & \sin\psi \end{bmatrix}, \tag{14}$$

is the transformation matrix that leads from the body frame to the inertial frame.

The equations of motion are developed using the Euler–Lagrange approach, i.e.,

$$\frac{d}{dt}\frac{\partial \mathcal{L}}{\partial \dot{\mathbf{q}}} - \frac{\partial \mathcal{L}}{\partial \mathbf{q}} = \mathbf{F}, \tag{15}$$

where the Lagrangian is written as the sum of translational and rotational kinetic energy

$$\mathcal{L} = \mathcal{K}_{tr} + \mathcal{K}_{rot} = \frac{1}{2}m(\dot{x}^2 + \dot{y}^2) + \frac{1}{2}I_{zz}\dot{\psi}^2, \tag{16}$$

and the generalized coordinate vector is defined as

$$\mathbf{q} = [x \quad y \quad \psi]^T, \tag{17}$$

where x and y represent the position and ψ represents the spin.

Applying (15), we obtain

$$\ddot{x} = \frac{1}{m}F_X, \tag{18}$$

$$\ddot{y} = \frac{1}{m}F_Y, \tag{19}$$

$$\ddot{\psi} = \frac{1}{I_{zz}}N, \tag{20}$$

where F_X and F_Y are the forces represented in the inertial frame. These forces are obtained as

$$\begin{bmatrix} F_X \\ F_Y \end{bmatrix} = \begin{bmatrix} -\sin\psi & \cos\psi \\ \cos\psi & \sin\psi \end{bmatrix} \begin{bmatrix} f_x \\ f_y \end{bmatrix} = \begin{bmatrix} -f_x\sin\psi + f_y\cos\psi \\ f_x\cos\psi + f_y\sin\psi \end{bmatrix}, \tag{21}$$

when applying the transformation matrix. The inertia product I_{zz} is obtained as

$$I_{zz} = \sum_{i=1}^{i=2} m_i r_i^2 = m_1 l^2 + m_2 l^2 = (m_1 + m_2)l^2 = ml^2, \tag{22}$$

where the mass of each plane is considered to be equal and m is their sum.

Then, the equations of motion are written as

$$\ddot{x} = \frac{1}{m}(-f_x \sin\psi + f_y \cos\psi), \tag{23}$$

$$\ddot{y} = \frac{1}{m}(f_x \cos\psi + f_y \sin\psi), \tag{24}$$

$$\ddot{\psi} = \frac{1}{I_{zz}}(lT_1 \cos(\mu) + lT_2 \cos(\mu)), \tag{25}$$

4. Control Strategy

The system consists of two fixed-wing aircraft that are connected by a rigid rod, as shown in Figure 2. The arrangement of airplanes causes a circular motion. This configuration forms a larger vehicle that resembles a single rotor, and its CM is assumed to be at the center of the two-aircraft system.

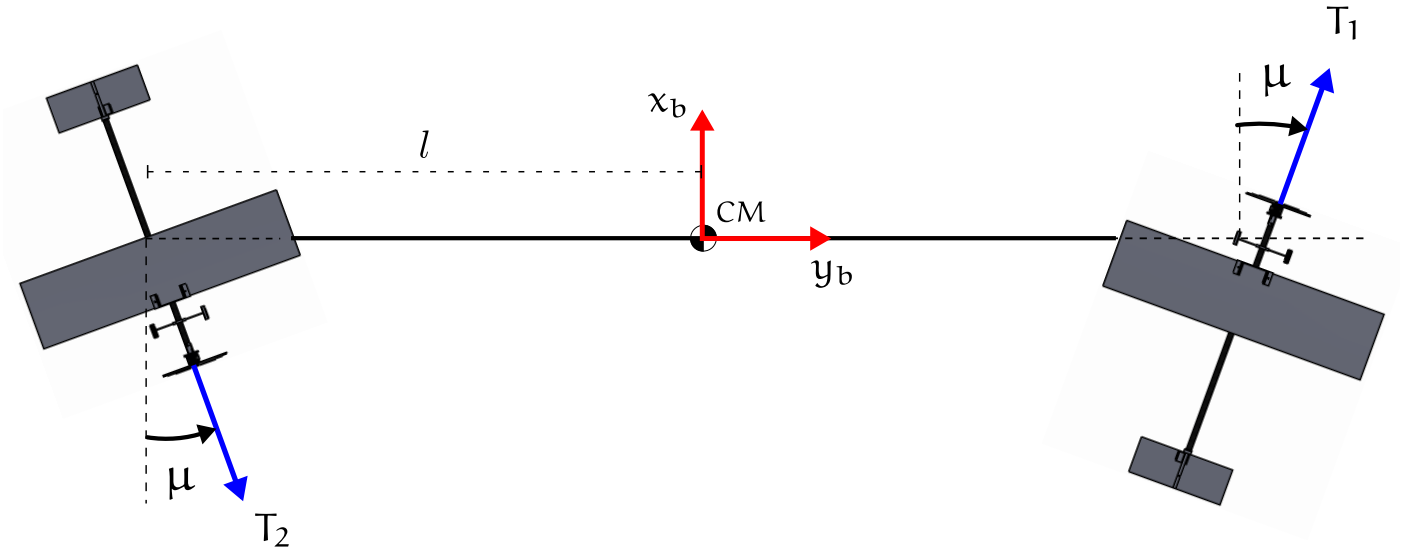

Figure 2. Rotating motion of the two airplanes.

4.1. Cyclic PD Control

The angular velocity control varies the thrust force of the motors simultaneously so that the control signal for each motor is

$$\tau_\psi = k_\psi(\dot{\psi}_d - \dot{\psi}) = k_\psi \dot{e}_\psi, \tag{26}$$

where k_ψ is a positive constant and $\dot{\psi}_d$ is the desired angular velocity.

The position control uses the aircraft engines to generate a varying thrust force; for this purpose, a cyclically varying proportional derivative control is chosen. The control signal in each motor for the displacement in the x-axis is set to

$$u_{1_x} = +k_1 e_x \sin(\psi) + k_{d1}\dot{e}_x \sin(\psi) = (k_1 e_x + k_{d1}\dot{e}_x)\sin(\psi), \tag{27}$$

$$u_{2_x} = -k_1 e_x \sin(\psi) - k_{d1}\dot{e}_x \sin(\psi) = (-k_1 e_x - k_{d1}\dot{e}_x)\sin(\psi), \tag{28}$$

and the signal for the displacement on the y-axis is

$$u_{1_y} = -k_2 e_y \cos(\psi) - k_{d2}\dot{e}_y \cos(\psi) = (-k_2 e_y - k_{d2}\dot{e}_y)\cos(\psi), \tag{29}$$

$$u_{2_y} = +k_2 e_y \cos(\psi) + k_{d2}\dot{e}_y \cos(\psi) = (k_2 e_y + k_{d2}\dot{e}_y)\cos(\psi), \tag{30}$$

where k_1 and k_2 are positive constants, while e_x and e_y are the positional errors defined as

$$e_x = x_d - x, \tag{31}$$

$$e_y = y_d - y, \tag{32}$$

where x_d and y_d are the coordinates of the desired position.

The system (27) and (28) control the displacement in the x-axis, which allows the magnitude of the proportional derivative control to be modulated. Due to the geometrical arrangement of the system, when the angle ψ is zero degrees, the thrust vector in the motors are aligned with the inertial y-axis, so in this configuration, no thrust is generated by the controller, but as the angle ψ increases, so does the value of the PD control. The ψ value increases so that when the value reaches 90°, the controller registers a maximum pulse; at this instant, the thrust vector is aligned with the inertial x-axis. After the maximum pulse is presented, the magnitude of the controller starts to decrease as ψ approaches 180°; when it reaches 180°, the thrust vector is again parallel to the y-axis where the value of the controller becomes zero. This behavior continues as the airplanes turn, so that when 270° is reached, the magnitude of the control has another maximum and subsequently becomes zero when the angle reaches 360°; thus, the dynamics is repeated with each turn the airplanes complete. This dynamics is achieved by multiplying the value of the PD control by a sinusoidal function that has ψ as argument; hence, it has been named as cyclic control or cyclic PD.

Similar behavior is obtained for Equations (29) and (30), which control the displacement in the y-axis. In this case, a cosine function with argument ψ is used, which multiplies the PD control.

Considering the above equations, we obtain the control signal for each actuator as

$$T_1 = \tau_\psi + u_{1_x} + u_{1_y}, \tag{33}$$

$$T_2 = \tau_\psi + u_{2_y} + u_{2_y}, \tag{34}$$

or equivalently

$$\begin{bmatrix} T_1 \\ T_2 \end{bmatrix} = \begin{bmatrix} k_\psi \dot{e}_\psi \\ k_\psi \dot{e}_\psi \end{bmatrix} + \begin{bmatrix} k_1 & k_{d_1} \\ -k_1 & -k_{d_1} \end{bmatrix} \begin{bmatrix} e_x \\ \dot{e}_x \end{bmatrix} \sin\psi + \begin{bmatrix} -k_2 & -k_{d_2} \\ k_2 & k_{d_2} \end{bmatrix} \begin{bmatrix} e_y \\ \dot{e}_y \end{bmatrix} \cos\psi, \tag{35}$$

where these signals indicate the revolutions on each motor to obtain the thrust force required to bring the system to the desired position.

4.2. Positive Function

This section presents a control strategy based on a positive function to regulate the displacement of the planes in the x–y plane. Equations of force in the body (2) are taken into account, and it is considered that $\mu = 0$, resulting in

$$f_x = T_1 - T_2, \tag{36}$$

$$f_y = 0. \tag{37}$$

Therefore, (21) for inertial force simplifies to

$$\begin{bmatrix} F_X \\ F_Y \end{bmatrix} = \begin{bmatrix} -f_x \sin\psi \\ f_x \cos\psi \end{bmatrix}, \tag{38}$$

hence, the system (23)–(25) reduces to

$$\ddot{x} = -\frac{1}{m}(f_x \sin\psi), \tag{39}$$

$$\ddot{y} = \frac{1}{m}(f_x \cos\psi), \tag{40}$$

$$\ddot{\psi} = \frac{1}{I_{zz}}(lT_1 + lT_2), \tag{41}$$

Then, the position control is set as

$$T_1 = \frac{1}{2}\frac{mI_{zz}}{I_{zz} - m\alpha_\psi l}F(\mathbf{p}), \tag{42}$$

$$T_2 = \frac{1}{2}\frac{mI_{zz}}{-I_{zz} - m\alpha_\psi l}F(\mathbf{p}), \tag{43}$$

where

$$F(\mathbf{p}) = -\frac{\kappa}{2}W - \dot{\psi}\cos(\psi)r_x + \dot{\psi}\sin(\psi)r_y - \sin(\psi)\alpha_x\dot{e}_x - \cos(\psi)\alpha_y\dot{e}_y, \tag{44}$$

$$W = \sin(\psi)r_x + \cos(\psi)r_y + r_\psi, \tag{45}$$

were obtained using a positive function approach; see Appendix A.

5. Numerical Simulation Results

5.1. Simulation Results Using the Cyclic PD

Simulation results of implementing the control strategies developed in the previous sections are presented below. The physical–geometric parameters of the system are listed in Table 1. These parameters correspond to a real vehicle, the air density at an altitude of 2240 m (Mexico city altitude) was set according to the ISA model.

Table 1. Physical parameters.

Parameter	Value
m	1 kg
l	1 m
Izz	1 kg · m^2
ρ	0.982428 kg/m^3
D	0.1016 m

The values of the parameters and initial conditions employed in the simulations are presented in Tables 2 and 3.

Table 2. Simulation parameters.

Parameter	Value
x_d	0.5 m
y_d	−0.5 m
$x(0)$	0 m
$y(0)$	0 m
$\psi(0)$	0 rad
$\dot{x}(0)$	0 m/s
$\dot{y}(0)$	0 m/s
$\dot{\psi}(0)$	0 rad/s
μ	0°–15°, 15°–0°

Table 3. Control parameters.

Parameter	Value
k_ψ	3200
k_1	2300
k_{d1}	1100
k_2	1500
k_{d2}	1100

Figure 3 shows the trajectory of each airplane. Since they start from the initial condition until they reach the desired point, the airplanes move describing a circumference that moves along the x–y plane. The trajectory of the center of gravity (CG) of the rotating system is shown in Figure 4; this trajectory shows an oscillating behavior when approximating the desired position, which is due to the nature of the vehicle. Figure 5 shows the norm of x–y position states; this norm tends to zero, which is evidence that the desired position is reached in a given time.

Figure 6 shows the evolution of the yaw angle of the planes as a function of time from the starting point (initial conditions of the simulation) up to the final or desired point. Finally, Figure 7 shows the forces acting on each motor; it can be appreciated that there exists a sinusoidal effect due to the sinusoidal control employed. From the figures, it can be noticed that the position control starts to act until the angular velocity is close to its desired value.

The variable μ is used as a static parameter and not as a control input, so this parameter is set manually, as shown in Figure 8. The value of μ changes with time from zero degrees up to fifteen degrees, stays at fifteen degrees for a while and then drops back down to zero degrees. The variation of this parameter causes the system to deviate considerably from its desired value; subsequently, the control counteracts the deviation until the position error decreases to zero, as shown in Figure 9. These error signals make also evident a sinusoidal behavior due to the applied control.

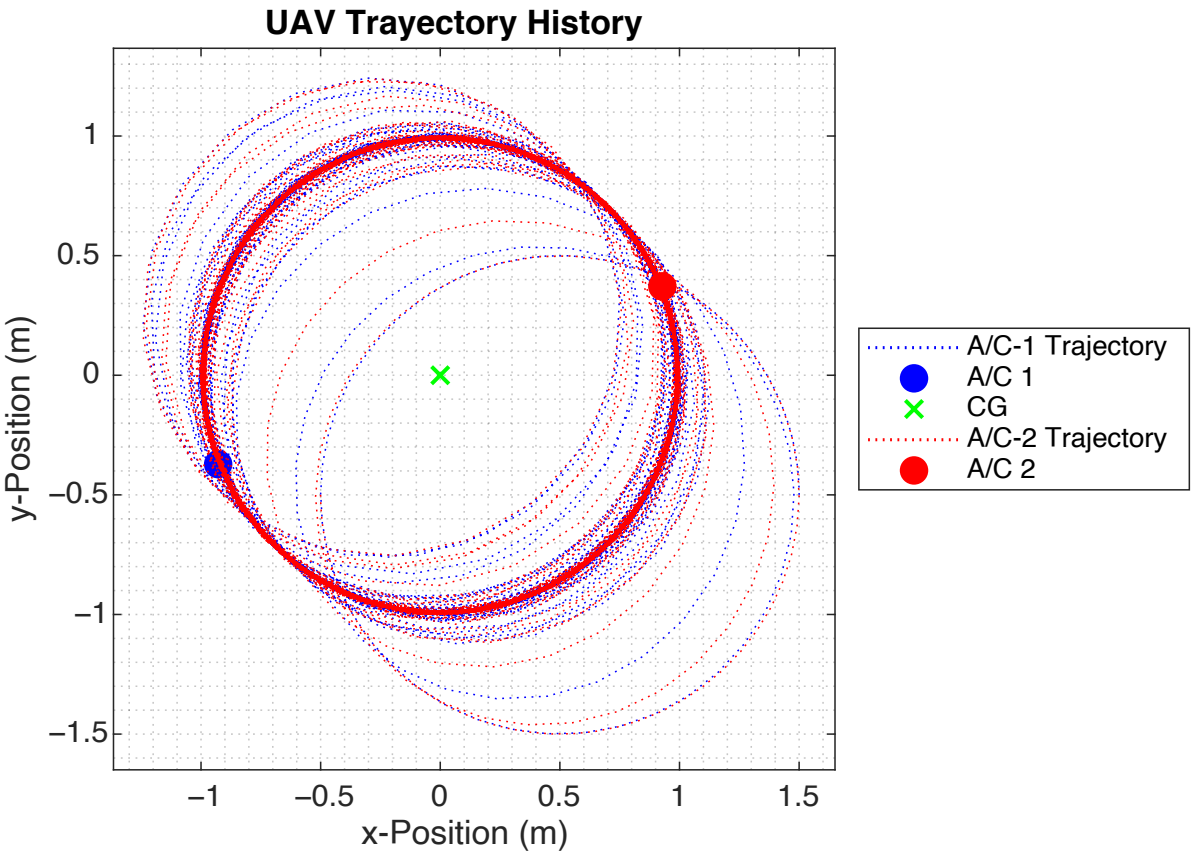

Figure 3. System trajectory.

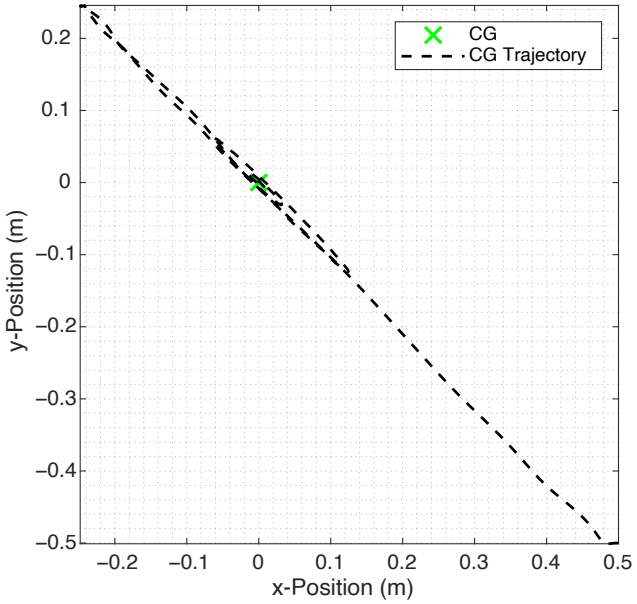

Figure 4. Motion of the CM.

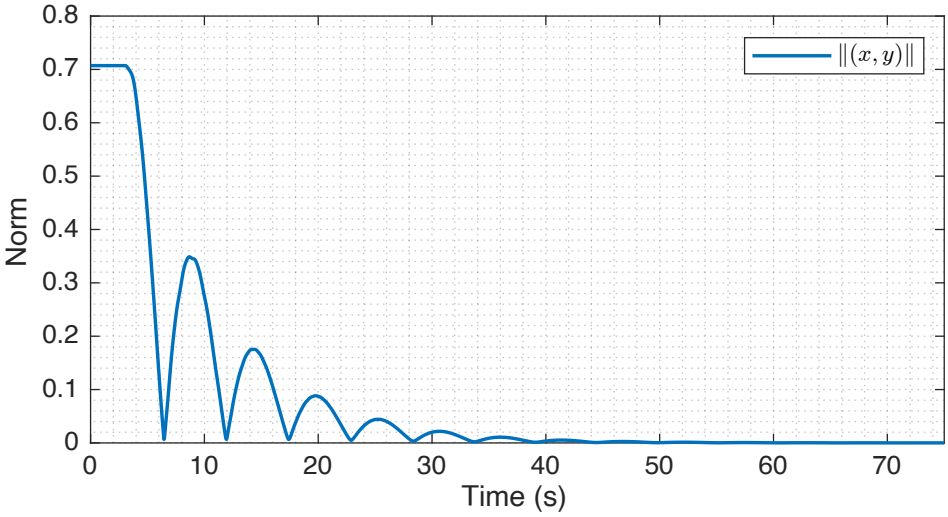

Figure 5. State Norm.

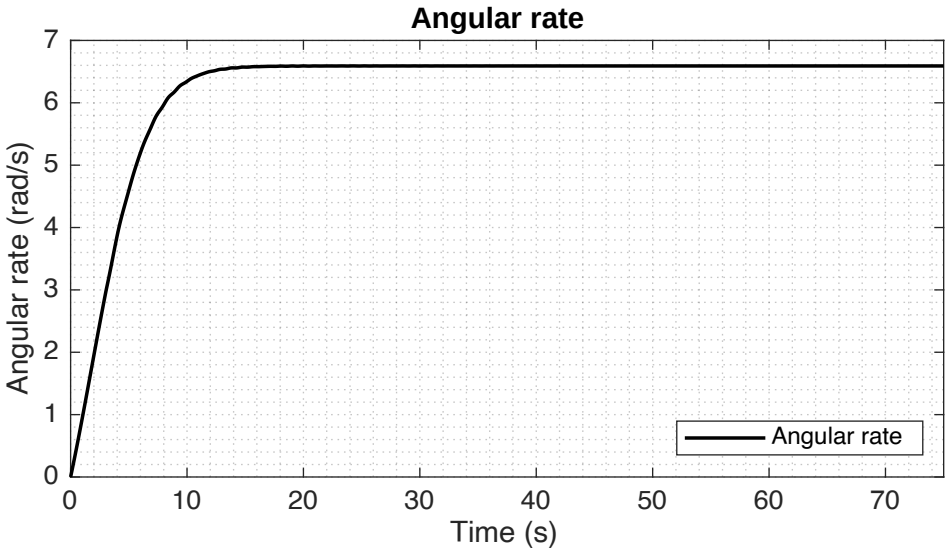

Figure 6. Angular yaw rate.

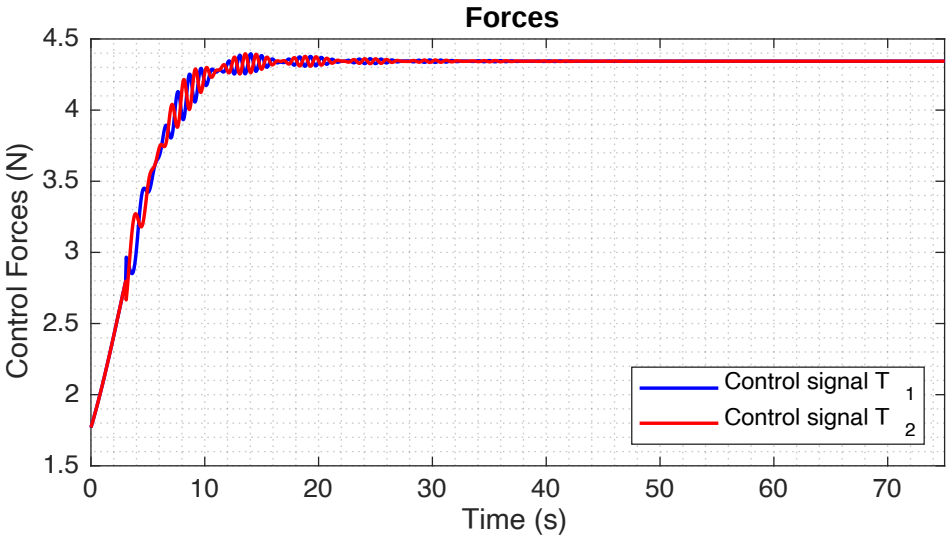

Figure 7. Thrust forces on each aircraft.

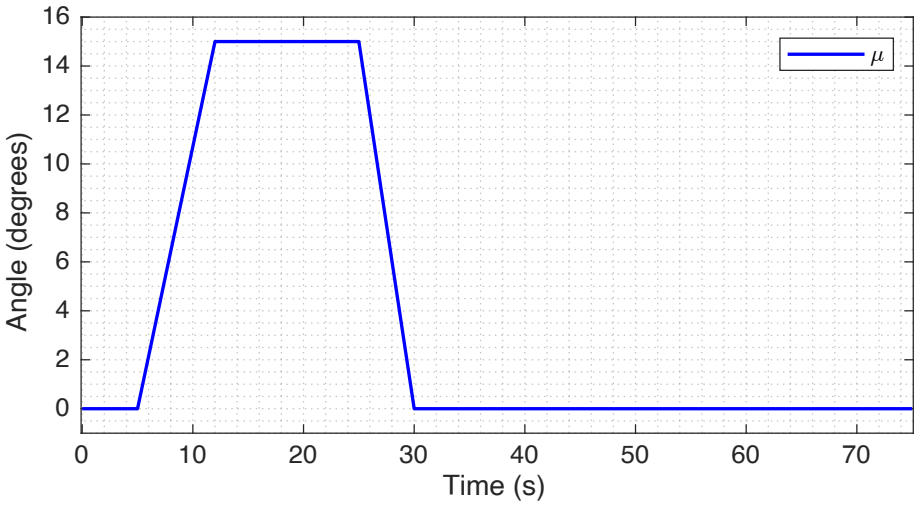

Figure 8. Variation of the μ angle.

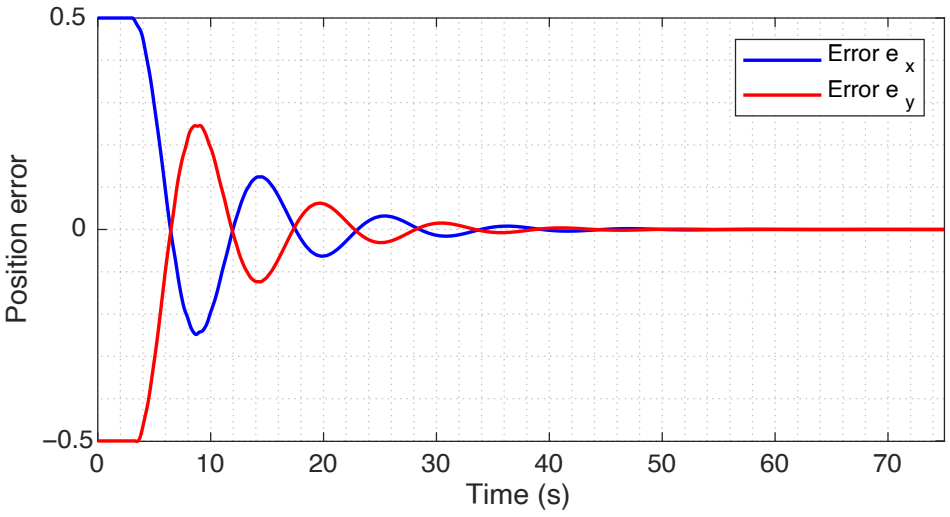

Figure 9. Position errors.

5.2. Simulation Results Using the Positive Function

The physical–geometric parameters of the system considered for this analysis are listed in Tables 4–6.

Table 4. Physical parameters.

Parameter	Value
m	1 kg
l	1 m
Izz	1 kg · m^2

Table 5. Values of the simulation parameters.

Parameter	Value
x_d	0 m
y_d	0 m
$\dot{\psi}_d$	6.5 rad/s
$x(0)$	0.5 m
$y(0)$	0.5 m
$\psi(0)$	0 rad
$\dot{x}(0)$	0 m/s
$\dot{y}(0)$	0 m/s
$\dot{\psi}(0)$	0 rad/s

Table 6. Values of the control parameters.

Parameter	Value
α_x	0.5
α_y	0.5
α_ψ	1.7
κ	2.0

The following figures show the behavior of the system when the positive function is applied. Figure 10 shows the trajectory of the UAV in the x–y plane where its CG is represented by a cross (X). The trajectories of the planes are represented by dotted lines. The blue and red dotted lines correspond to the A/C 1 and A/C 2 planes, respectively. As expected, the trajectories are circular from the initial to the final desired position. Figure 11 corresponds to the same motion of the vehicle; the figure registers the trajectory of the CG of the vehicle. Figure 12 shows the norm of x–y position states, the decreasing behavior points to the conclusion that in finite time, the vehicle approaches the desired position. Figure 13 shows the evolution of the yaw angle rate of the system with respect to time; it can be observed how the control regulates the angular velocity until the reference value is reached. The actuating forces of each motor are shown in Figure 14; these control signals allow the vehicle to regulate its position and its angular speed. Finally, the convergence of the position error is shown in Figure 15, where an oscillating and decreasing behavior of it can be observed leading to the conclusion that it vanishes.

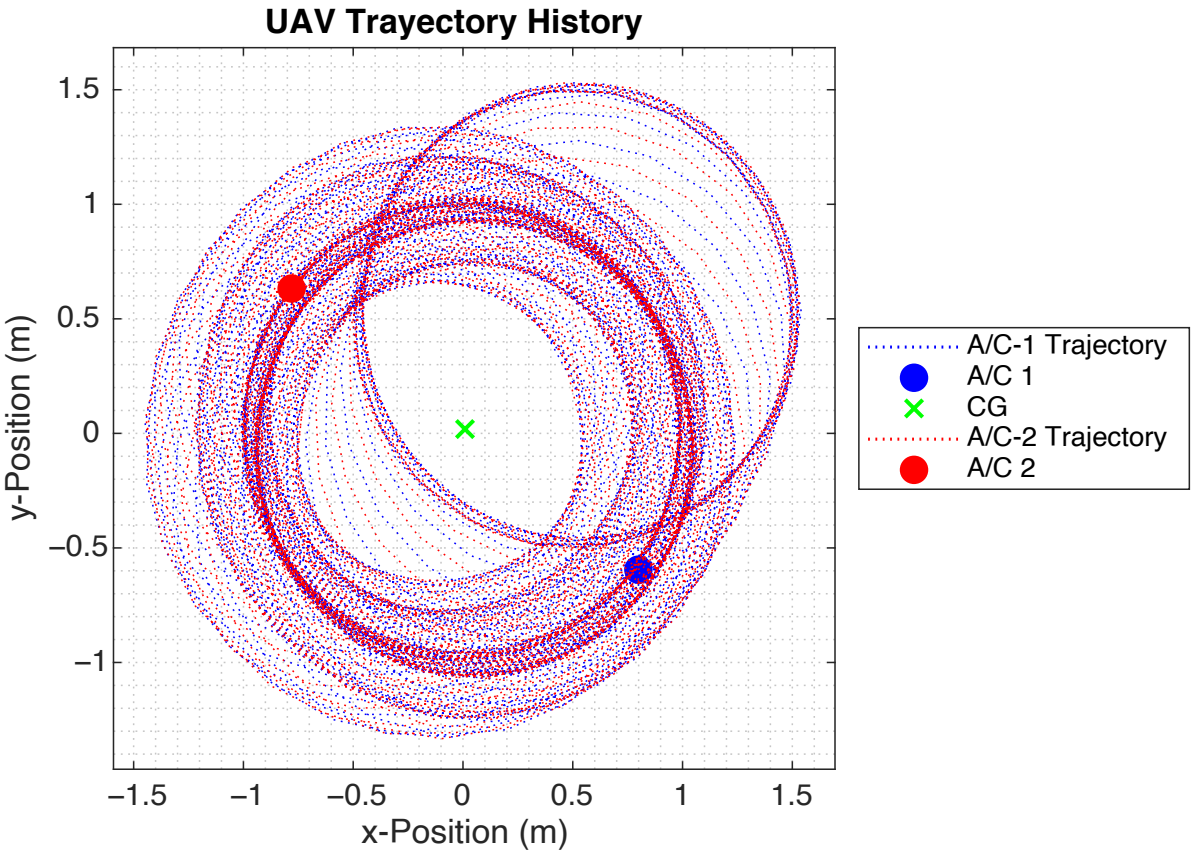

Figure 10. UAV Trajectory.

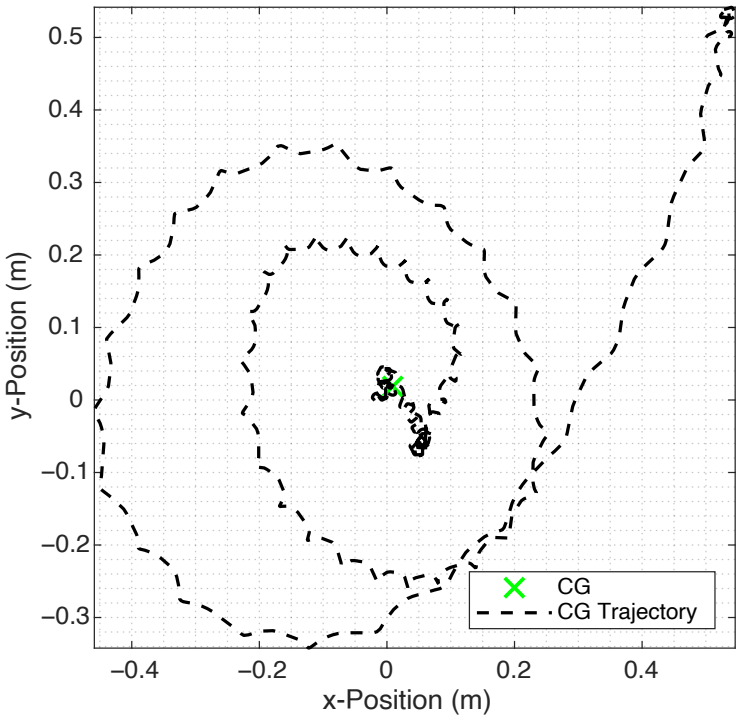

Figure 11. Motion of the centre of mass.

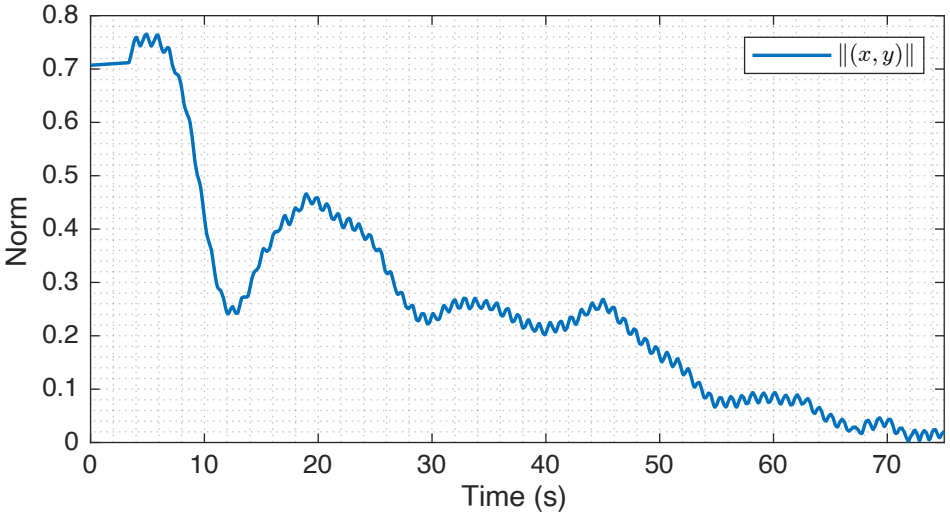

Figure 12. Norm of the states.

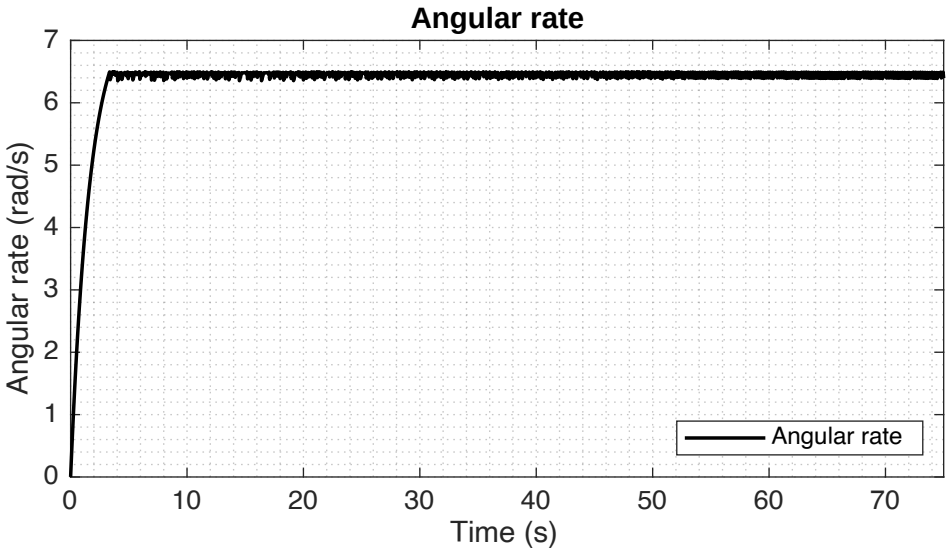

Figure 13. Angular yaw rate.

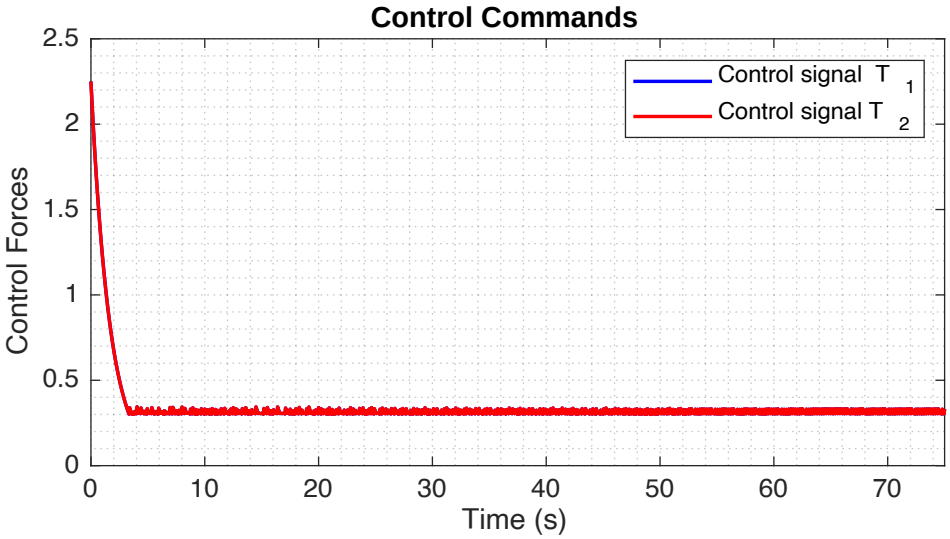

Figure 14. Control signals.

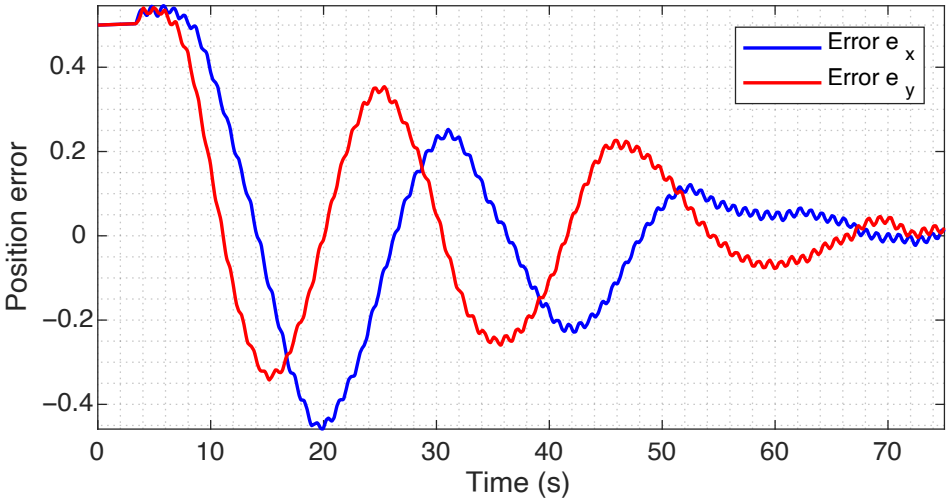

Figure 15. Position errors.

Comparison of the Two Controllers

Figure 16 shows the comparison of the norm of the position states for both controls, positive function and cyclic PD. Both controllers have a similar response, this is due to the sinusoidal nature of the controls that lead to an oscillating behavior observed in the dynamic position of the vehicle. The controls successfully placed the vehicle in the desired position; this can be verified watching the decreasing behavior of the norm.

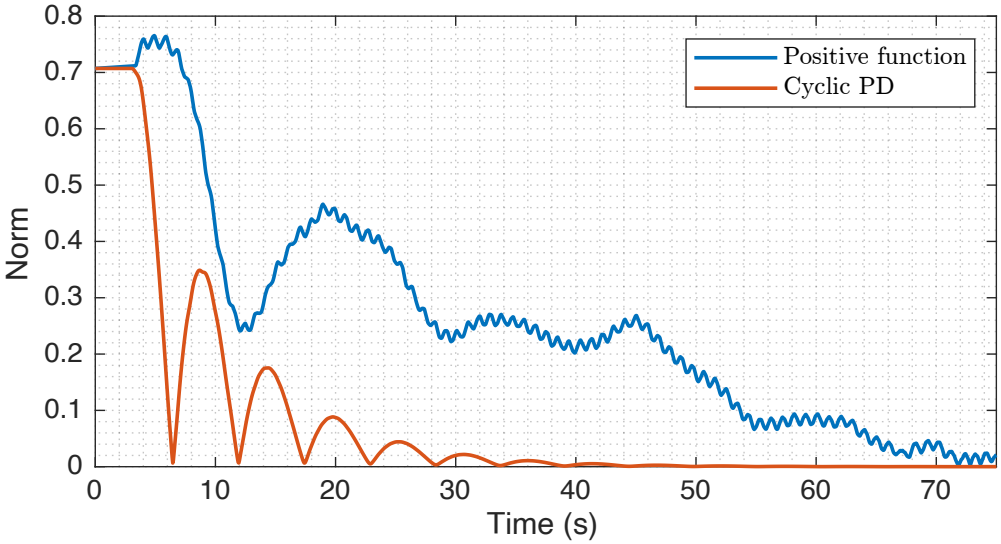

Figure 16. Comparison of the norm of the two controls.

6. Conclusions

This paper has presented two control techniques to control the horizontal displacement of a set of two attached rotating airplanes. One of them uses a PD control that varies cyclically, and the other one uses a positive function approach. The rotating aircraft were modeled using the Euler–Lagrange approach, and numerical simulations showed the effectiveness of control techniques. Even though the rudder and elevator of each airplane are installed, only the thrust force was used for control.

In order to achieve horizontal movements of the prototype, we created a virtual swashplate to emulate this mechanism in helicopters. The virtual swashplate was created by introducing a sinusoidal control on the airplanes' motors. The thrust amplitude was proportional to the sinusoidal amplitude, and the direction was determined by the phase of the introduced sinusoidal signal.

Nonlinear control algorithms enabled the rotating airplanes to reach a particular position in space. The performance of the control strategies was compared and successfully tested in numerical simulations.

Future research will include the vertical take off and landing stages of the vehicle. The transition from the vertical take off to the cruise flight and vice versa from the cruise flight to the vertical landing stage will also be considered. Another future topic of research will include an experimental study of the control behavior of Euler angles when the proposed strategy is the usage of the elevators of the planes as actuators. The control of the horizontal displacement will also be studied considering a power difference of the motors of the planes or a difference in the position of the rudders.

Author Contributions: Conceptualization, investigation, writing—original draft preparation, J.A.B.-M.; Methodology, writing—review and editing, R.L.; Validation, supervision, A.O.-C. All authors have read and agreed to the published version of the manuscript.

Funding: This research was funded by CONACYT of Mexico through project 314879 "Laboratorio Nacional en Vehiculos Autonomos y Exoesqueletos LANAVEX". The lead author was also supported by the UMI-LAFMIA CINVESTAV Mexico Preeminent Doctoral Program.

Institutional Review Board Statement: Not applicable.

Informed Consent Statement: Not applicable.

Data Availability Statement: Not applicable.

Conflicts of Interest: The authors declare no conflict of interest. The funders had no role in the design of the study; in the collection, analyses, or interpretation of data; in the writing of the manuscript, or in the decision to publish the results.

Abbreviations

The following abbreviations are used in this manuscript:

A/C	Aircraft
CG	Center of gravity
CM	Center of mass
ISA	International Standard Atmosphere
PD	Proportional derivative
UAV	Unmanned Aerial Vehicle

Appendix A. Deduction of Control Using a Positive Function

Let be the system defined by the Equations (39)–(41). The state vector and state variables are defined as

$$\mathbf{p} = \begin{bmatrix} p_1 & p_2 & p_3 & p_4 & p_5 & p_6 \end{bmatrix}^T = \begin{bmatrix} x & \dot{x} & y & \dot{y} & \psi & \dot{\psi} \end{bmatrix}^T, \tag{A1}$$

differentiating the state variables, the following is obtained

$$\dot{p}_1 = p_2, \tag{A2}$$

$$\dot{p}_2 = -\frac{1}{m} f_x \sin(\psi), \tag{A3}$$

$$\dot{p}_3 = p_4, \tag{A4}$$

$$\dot{p}_4 = \frac{1}{m} f_x \cos(\psi), \tag{A5}$$

$$\dot{p}_5 = p_6, \tag{A6}$$

$$\dot{p}_6 = \frac{1}{I_{zz}} (lT_1 + lT_2), \tag{A7}$$

The desired state vector is defined as

$$\mathbf{p_d} = \begin{bmatrix} x_d & * & y_d & * & * & \dot{\psi}_d \end{bmatrix}^T, \tag{A8}$$

where * indicates that no value is set for that state. The following functions and error functions are defined

$$r_x = \dot{e}_x + \alpha_x e_x = (\dot{x}_d - \dot{x}) + \alpha_x (x_d - x), \tag{A9}$$
$$r_y = \dot{e}_y + \alpha_y e_y = (\dot{y}_d - \dot{y}) + \alpha_y (y_d - y), \tag{A10}$$
$$r_\psi = \alpha_\psi \dot{e}_\psi = \alpha_\psi (\dot{\psi}_d - \dot{\psi}), \tag{A11}$$
$$e_x = x_d - x, \tag{A12}$$
$$e_y = y_d - y, \tag{A13}$$
$$\dot{e}_\psi = \dot{\psi}_d - \dot{\psi}, \tag{A14}$$

where α_x, α_y and α_ψ are positive constants.

Set the positive function as

$$V(\mathbf{p}) = \frac{1}{2} W^2, \tag{A15}$$

where

$$W = \sin(\psi) r_x + \cos(\psi) r_y + r_\psi, \tag{A16}$$

then, Equation (A15) can be rewritten in vector form as

$$V(\mathbf{p}) = \frac{1}{2} \left(\begin{bmatrix} \sin(\psi) & \cos(\psi) & 1 \end{bmatrix} . \begin{bmatrix} r_x \\ r_y \\ r_\psi \end{bmatrix} \right)^2 = \frac{1}{2} (\mathbf{v_1 v_2})^2 \geq 0, \tag{A17}$$

where the vector $\mathbf{v_1}$ is a function of ψ which varies much faster than the vector $\mathbf{v_2}$, i.e., the variable ψ performs complete cycles from 0 to 360 degrees in a given amount of time while the functions r_x, r_y and r_ψ associated with the states x, y and $\dot{\psi}$ vary slowly as if they remained constant. This behavior is due to the way the vehicle moves, the CG moves slower compared to the rotation of the system (see Section 5). Therefore it is possible to choose values of ψ in a given cycle such that:

$$V_1(\mathbf{p})\Big|_{\psi=0} = \frac{1}{2} \left(\begin{bmatrix} 0 & 1 & 1 \end{bmatrix} . \begin{bmatrix} r_x \\ r_y \\ r_\psi \end{bmatrix} \right)^2, \tag{A18}$$

$$V_4(\mathbf{p})\Big|_{\psi=1/2\pi} = \frac{1}{2} \left(\begin{bmatrix} 1 & 0 & 1 \end{bmatrix} . \begin{bmatrix} r_x \\ r_y \\ r_\psi \end{bmatrix} \right)^2, \tag{A19}$$

$$V_6(\mathbf{p})\Big|_{\psi=\pi} = \frac{1}{2} \left(\begin{bmatrix} 0 & -1 & 1 \end{bmatrix} . \begin{bmatrix} r_x \\ r_y \\ r_\psi \end{bmatrix} \right)^2, \tag{A20}$$

Since V(p) in (A17) converges to zero and using the above it follows:

$$\begin{bmatrix} 0 & 1 & 1 \\ 1 & 0 & 1 \\ 0 & -1 & 1 \end{bmatrix} . \begin{bmatrix} r_x \\ r_y \\ r_\psi \end{bmatrix} = 0 = \mathbf{C_1 r_1}, \tag{A21}$$

where the matrix $\mathbf{C_1}$ is regular with eigenvalues $\{1+i, 1-i, -1\}$ therefore the vector $\mathbf{v_1}$ will converge to zero.

Differentiating (A15) respect to time the following is obtained

$$\dot{V}(\mathbf{p}) = W(\sin(\psi)\dot{r}_x + \dot{\psi}\cos(\psi)r_x + \cos(\psi)\dot{r}_y - \dot{\psi}\sin(\psi)r_y + \dot{r}_\psi), \tag{A22}$$

in order to achieve global exponential stability, it is required that (A23) is satisfied for $\kappa > 0$ see [12]

$$\dot{V}(\mathbf{p}) = -\kappa V, \tag{A23}$$

Therefore, the term in the parentheses furthest to the right of (A22) must satisfy the following

$$(\sin(\psi)\dot{r}_x + \dot{\psi}\cos(\psi)r_x + \cos(\psi)\dot{r}_y - \dot{\psi}\sin(\psi)r_y + \dot{r}_\psi) = -\frac{\kappa}{2}W, \tag{A24}$$

grouping $\dot{r}_x$, $\dot{r}_y$ and $\dot{r}_\psi$ and substituting their values the following is obtained

$$\sin(\psi)\dot{r}_x + \cos(\psi)\dot{r}_y + \dot{r}_\psi = -\frac{\kappa}{2}W - \dot{\psi}\cos(\psi)r_x + \dot{\psi}\sin(\psi)r_y, \tag{A25}$$

$$\sin(\psi)(\ddot{e}_x + \alpha_x\dot{e}_x) + \cos(\psi)(\ddot{e}_y + \alpha_y\dot{e}_y) + \alpha_\psi\dot{e}_\psi = -\frac{\kappa}{2}W - \dot{\psi}\cos(\psi)r_x + \dot{\psi}\sin(\psi)r_y, \tag{A26}$$

$$\begin{aligned}\sin(\psi)\ddot{e}_x + \cos(\psi)\ddot{e}_y + \alpha_\psi\dot{e}_\psi = \\ -\frac{\kappa}{2}W - \dot{\psi}\cos(\psi)r_x + \dot{\psi}\sin(\psi)r_y - \sin(\psi)\alpha_x\dot{e}_x - \cos(\psi)\alpha_y\dot{e}_y,\end{aligned} \tag{A27}$$

also if x_d, y_d and $\dot{\psi}_d$ are constant values, $\ddot{e}_x$, $\ddot{e}_y$ and $\ddot{e}_\psi$ are simplified, then (A27) becomes

$$\begin{aligned}\sin(\psi)(-\ddot{x}) + \cos(\psi)(-\ddot{y}) + \alpha_\psi(-\ddot{\psi}) = \\ -\frac{\kappa}{2}W - \dot{\psi}\cos(\psi)r_x + \dot{\psi}\sin(\psi)r_y - \sin(\psi)\alpha_x\dot{e}_x - \cos(\psi)\alpha_y\dot{e}_y,\end{aligned} \tag{A28}$$

$$\begin{aligned}\sin(\psi)(\frac{1}{m}f_x\sin(\psi)) + \cos(\psi)(\frac{1}{m}f_x\cos(\psi)) + \alpha_\psi(-\frac{l}{I_{zz}}(T_1+T_2)) = \\ -\frac{\kappa}{2}W - \dot{\psi}\cos(\psi)r_x + \dot{\psi}\sin(\psi)r_y - \sin(\psi)\alpha_x\dot{e}_x - \cos(\psi)\alpha_y\dot{e}_y,\end{aligned} \tag{A29}$$

$$\begin{aligned}\frac{1}{m}f_x(\sin^2(\psi) + \cos^2(\psi)) - \frac{\alpha_\psi l}{I_{zz}}(T_1+T_2) = \\ -\frac{\kappa}{2}W - \dot{\psi}\cos(\psi)r_x + \dot{\psi}\sin(\psi)r_y - \sin(\psi)\alpha_x\dot{e}_x - \cos(\psi)\alpha_y\dot{e}_y,\end{aligned} \tag{A30}$$

$$\begin{aligned}\frac{1}{m}(T_1 - T_2) - \frac{\alpha_\psi l}{I_{zz}}(T_1+T_2) = \\ -\frac{\kappa}{2}W - \dot{\psi}\cos(\psi)r_x + \dot{\psi}\sin(\psi)r_y - \sin(\psi)\alpha_x\dot{e}_x - \cos(\psi)\alpha_y\dot{e}_y,\end{aligned} \tag{A31}$$

grouping T_1 and T_2 the following is obtained

$$\begin{aligned}\frac{1}{m}T_1 - \frac{\alpha_\psi l}{I_{zz}}T_1 - \frac{1}{m}T_2 - \frac{\alpha_\psi l}{I_{zz}}T_2 = \\ -\frac{\kappa}{2}W - \dot{\psi}\cos(\psi)r_x + \dot{\psi}\sin(\psi)r_y - \sin(\psi)\alpha_x\dot{e}_x - \cos(\psi)\alpha_y\dot{e}_y,\end{aligned} \tag{A32}$$

$$\frac{I_{zz} - m\alpha_\psi l}{mI_{zz}} T_1 + \frac{-I_{zz} - m\alpha_\psi l}{mI_{zz}} T_2 =$$
$$-\frac{\kappa}{2} W - \dot{\psi}\cos(\psi) r_x + \dot{\psi}\sin(\psi) r_y - \sin(\psi)\alpha_x \dot{e}_x - \cos(\psi)\alpha_y \dot{e}_y, \tag{A33}$$

$$\frac{I_{zz} - m\alpha_\psi l}{mI_{zz}} T_1 + \frac{-I_{zz} - m\alpha_\psi l}{mI_{zz}} T_2 = F(\mathbf{p}), \tag{A34}$$

where

$$F(\mathbf{p}) = -\frac{\kappa}{2} W - \dot{\psi}\cos(\psi) r_x + \dot{\psi}\sin(\psi) r_y - \sin(\psi)\alpha_x \dot{e}_x - \cos(\psi)\alpha_y \dot{e}_y, \tag{A35}$$

From (A34) it can be seen that it is convenient to select

$$T_1 = \frac{1}{2} \frac{mI_{zz}}{I_{zz} - m\alpha_\psi l} F(\mathbf{p}), \tag{A36}$$

$$T_2 = \frac{1}{2} \frac{mI_{zz}}{-I_{zz} - m\alpha_\psi l} F(\mathbf{p}), \tag{A37}$$

as the controls that can be adjusted using the parameters α_x, α_y, α_ψ and κ. With this selection it is satisfied that $\dot{V}(\mathbf{p})$ in (A23) is negative definite as required for stability.

References

1. Sanchez-Rivera, L.M.; Lozano, R.; Arias-Montano, A. Development, Modeling and Control of a Dual Tilt-Wing UAV in Vertical Flight. *Drones* **2020**, *4*, 71. [CrossRef]
2. Bautista, J.A.; Osorio, A.; Lozano, R. Modeling and analysis of a tricopter/flying-wing convertible uav with tilt-rotors. In Proceedings of the 2017 International Conference on Unmanned Aircraft Systems (ICUAS), Miami, FL, USA, 13–16 June 2017; pp. 672–681.
3. Low, J.E.; Win, L.T.S.; Shaiful, D.S.B.; Tan, C.H.; Soh, G.S.; Foong, S. Design and dynamic analysis of a Transformable Hovering Rotorcraft (THOR). In Proceedings of the 2017 IEEE International Conference on Robotics and Automation (ICRA), Singapore, 29 May–3 June 2017; pp. 6389–6396.
4. Escareno, J.; Salazar, S.; Lozano, R. Modelling and Control of a Convertible VTOL Aircraft. In Proceedings of the 45th IEEE Conference on Decision and Control, San Diego, CA, USA, 13–15 December 2006; pp. 69–74.
5. Aktas, Y.O.; Ozdemir, U.; Dereli, Y.; Tarhan, A.F.; Cetin, A.; Vuruskan, A.; Yuksek, B.; Cengiz, H.; Basdemir, S.; Ucar, M.; et al. Rapid Prototyping of a Fixed-Wing VTOL UAV for Design Testing. *J. Intell. Robot. Syst.* **2016**, *84*, 639–664. [CrossRef]
6. Garcia, O.; Castillo, P.; Wong, K.C.; Lozano, R. Attitude Stabilization with Real-time Experiments of a Tail-sitter Aircraft in Horizontal Flight. *J. Intell. Robot. Syst.* **2012**, *65*, 123–136. [CrossRef]
7. Venkatesan, C. *Fundamentals of Helicopter Dynamics*; CRC Press: Boca Raton, FL, USA, 2015.
8. Impulse, S. Solar Impulse Foundation: 1000 Profitable Solutions for the Environment. Available online: https://solarimpulse.com/ (accessed on 1 April 2021).
9. Bautista-Medina, J.A.; Lozano, R.; Osorio-Cordero, A. Modeling and Control of a Single Rotor Composed of Two Fixed Wing Airplanes. *Drones* **2021**, *5*, 92. [CrossRef]
10. McCormick, B.W. *Aerodynamics, Aeronautics, and Flight Mechanics*, 2nd ed.; Wiley: New York, NY, USA, 1995.
11. Brandt, J.B.; Deters, R.W.; Ananda, G.K.; Dantsker, O.D.; Selig, M.S. UIUC Propeller Database, Vols 1–3. Available online: https://m-selig.ae.illinois.edu/props/propDB.html (accessed 1 March 2022).
12. Isidori, A. *Nonlinear Control Systems*, 3rd ed.; Communications and Control Engineering Series; Springer: Berlin, Germany; New York, NY, USA, 1995.